Journal of Petroleum Science and Engineering 177 (2019) 880–888

Contents lists available at ScienceDirect

Journal of Petroleum Science and Engineering

journal homepage: www.elsevier.com/locate/petrol

Measurements of CH_4 and CO_2 relative permeability in hydrate-bearing sandstone

Stian Almenningen[a,*], Jarand Gauteplass[b], Lars Petter Hauge[a], Tanja Barth[b], Martin Anders Fernø[a], Geir Ersland[a]

[a] Department of Physics and Technology, University of Bergen, Norway
[b] Department of Chemistry, University of Bergen, Norway

ARTICLE INFO

Keywords:
CH_4 and CO_2 hydrates
Relative permeability
Effect of hydrate saturation

ABSTRACT

This paper reports measurements of relative permeability to methane (CH_4) and carbon dioxide (CO_2) in hydrate-bearing sandstone core samples. The CH_4 (or CO_2) permeability was measured at reservoir conditions for different hydrate and brine saturations. The saturation span ranged from 0.18 to 0.60 (frac.) for CH_4 gas and from 0.37 to 0.70 (frac.) for liquid CO_2. The hydrate saturation ranged from 0.18 to 0.61 (frac.). The growth of hydrates within sandstone pores reduced the permeability for both the CH_4 and CO_2 system significantly, and the relative reduction was more pronounced for lower gas saturations. This effect is currently not included in numerical models of relative permeability in hydrate-bearing sediments and should be considered. The reported measurements are relevant to production-forecasting of methane gas from hydrate reservoirs and CO_2 storage schemes where CO_2 hydrates may provide self-sealing in cold aquifers.

1. Introduction

Natural gas hydrates can be a nuisance and hazard in gas production and pipeline transport but are also recognized as a promising energy resource for the future. The crystalline compound, formed by hydrogen-bonded water molecules and stabilized by methane (CH_4) molecules, is distributed worldwide in shallow marine sediments and onshore in and below permafrost. Global estimates range from 10^{14} – 10^{18} Sm^3 of entrapped CH_4 gas in natural gas hydrates (Milkov, 2004). Several short-term field pilots (Dallimore et al., 2012; Schoderbek et al., 2012; Yamamoto et al., 2014) have been undertaken but the longer term dynamics of CH_4 production from natural gas hydrate reservoirs remain unclear. Relative permeability functions in hydrate-bearing sediments are key input to model flow and assess the production performance in any production scheme (Moridis et al., 2007; Reagan et al., 2008). Understanding hydrate dissociation pattern and, in turn, the mobilization of gas and water in sedimentary systems is vital to predict long-term production rates (Jang and Santamarina, 2014).

Gas hydrates form with several other small non-polar guest molecules than CH_4 and carbon dioxide (CO_2) is particularly interesting. CO_2 hydrates are thermodynamically more stable than CH_4 hydrates which will induce a spontaneous exchange of the hydrate guest and release CH_4 gas to be produced (Graue et al., 2008). CO_2 hydrates may also aid as an extra sealing for CO_2 storage in cold aquifers (Kvamme et al., 2007). Fluxes of buoyant CO_2 will be significantly reduced by the formation of CO_2 hydrates in the pore space (Tohidi et al., 2010). In order to model the strength and effectiveness of the formed CO_2 hydrate seal, the relationship between CO_2 permeability and CO_2 hydrate saturation must be known. In this case, a critical CO_2 hydrate saturation will immobilize the injected CO_2, whereas from a production point of view a critical CH_4 hydrate saturation will determine when CH_4 gas starts flowing. In either way, it is important to identify the transition in hydrate saturation where the fluids become stationary (Seol and Kneafsey, 2011).

Measuring the permeability of hydrate-saturated porous media is not straightforward as opposed to conventional two-phase flow. The action of performing a permeability measurement will affect the stability of the hydrate system and thereby the permeability itself. When the pore space is partly occupied by gas hydrates, injection of gas or water are typically modelled as regular two-phase flow, where the effective porosity and absolute permeability are functions of the hydrate saturation (Moridis and Pruess, 2014). However, the solid hydrate phase is susceptible for changes during the flow measurement, e.g. hydrate may form, redistribute or dissociate as water and gas are mixed during two-phase flow (Johnson et al., 2011). In the case where the pore space is filled with hydrates and water (containing dissolved

* Corresponding author.
E-mail address: stian.almenningen@uib.no (S. Almenningen).

https://doi.org/10.1016/j.petrol.2019.02.091
Received 3 December 2018; Received in revised form 25 February 2019; Accepted 28 February 2019
Available online 05 March 2019
0920-4105/

hydrate former), injection of undersaturated water leads to scavenging of the dissolved guest molecule from the system (Delli and Grozic, 2014) and subsequent hydrate dissociation. Thermal non-equilibrium effects may also be significant if the injected fluid is not properly cooled before injection, depending on the applied flow rate and temperature control. The pore-scale distribution of hydrates affects the permeability severely independent of the hydrate saturation (Kleinberg et al., 2003). The permeability also depends on the macroscopic distribution of hydrates, as hydrates formed in large patchy clusters exhibit higher permeability compared to distributed hydrates (Mahabadi et al., 2019). The pore-scale hydrate distribution is often simply considered as either grain-coating or pore-filling depending on the initial fluid distribution and choice of hydrate formation method (Kleinberg et al., 2003). One study suggests that the hydrate distribution changes from mineral coating to pore center filling when the hydrate saturation is increased above 35% (Kumar et al., 2010). The effect of hydrate saturation on the relative permeability to gas is also shown to differ when different porous media is used (Jaiswal et al., 2009), and anisotropic permeability values were found when the effect of applied stress to the core sample was investigated, showing the importance of differentiating between horizontal and vertical permeability in the field (Dai et al., 2018). The abovementioned issues related to obtaining the permeability of hydrate-bearing sediments give rise to a scattered range of results in the literature. The end-point relative permeability to gas has been measured to be less than 0.01 ($S_H \approx 0.13$, $S_g \approx 0.26$ and $S_w \approx 0.61$) in one study (Johnson et al., 2011) and approximately 0.1 ($S_H \approx 0.15$, $S_g \approx 0.28$, $S_w \approx 0.57$) in another (Ahn et al., 2005). Johnson et al. (2011) used nitrogen gas to obtain gas-water relative permeability curves because of severe secondary hydrate formation when CH_4 was injected, contrary to Ahn et al. (2005) and Jaiswal et al. (2009) which did not experience plugging during unsteady state permeability measurements with CH_4 gas. The disadvantage with using nitrogen gas is that the displacement of CH_4 gas will likely destabilize the CH_4 hydrate.

The scope of this work is to compare the relative permeability to CH_4 gas in CH_4 hydrate saturated sandstone with the relative permeability to liquid CO_2 in CO_2 hydrate saturated sandstone. The solubility of CO_2 in water (Servio and Englezos, 2001) is approximately one order of magnitude higher than the solubility of CH_4 in water (Servio and Englezos, 2002), which may yield different hydrate growth patterns and possibly different relative permeability functions. The limiting CH_4 (or CO_2) saturation where the apparent permeability of the hydrate-filled pore space drops to zero is identified for both hydrate formers. The permeability values obtained in this study can be used as input to numerical simulators, especially in schemes trying to model the production of hydrate-bound CH_4 gas by CO_2 injection. The long-term prediction of CH_4 gas production from hydrate must incorporate the change in fluid permeability as the hydrate saturation decreases through dissociation.

2. Materials and methods

2.1. Establishing initial brine saturation

Cylindrical Bentheim sandstone core plugs with nominal porosity of 0.24 (frac.) and absolute permeability of 1.1–1.9 Darcy (detailed in Table 1) were used as analogues to reservoir rock. The core plugs were partially saturated with brine by one of three methods to create a range in initial water saturation and distribution in the core: A) a fully brine saturated core plug (initially air evacuated and filled with brine under vacuum) was partially saturated with gaseous CO_2 at ambient conditions by injecting at a constant pressure drop of ~0.3 MPa; B) a dry core plug was submerged in brine for a limited time (10–20 s) to allow brine to invade the pore space by spontaneous imbibition; or C) a fully brine saturated core plug was wrapped in wiping paper and subjected to a vacuum (P ~ 100 Pa) for 10–20 s to remove brine from the pore space. Average brine saturations were quantified by weight calculations and spatial distributions of brine were quantified and visualized using magnetic resonance imaging (MRI). The distribution of initial brine in the core was later used to aid the interpretation of the permeability measurements.

Table 1
Core plug properties and initial saturation of brine. Every core plug was ~15 cm long with a diameter of ~5 cm. Margin of errors reflect instrumental uncertainties. *The absolute permeability was not measured in this core plug and the given value is the midpoint of the other permeability values.

Core ID	Φ (frac.) ± 0.01	K_{abs} (D)	Saturation method	S_{wi} (frac.) ± 0.01	Brine salinity (wt% NaCl) ± 0.01
CO2_base	0.23	1.11 ± 0.07	–	1	3.50
CO2_1	0.24	*1.5 ± 0.1	A	0.27	0.10
CO2_2	0.24	1.45 ± 0.03	B	0.34	0.10
CO2_3	0.24	*1.5 ± 0.1	B	0.40	0.10
CO2_4	0.24	1.53 ± 0.04	B	0.40	0.10
CO2_5	0.24	*1.5 ± 0.1	B	0.43	0.10
CO2_6	0.24	*1.5 ± 0.1	B	0.44	0.10
CO2_7	0.24	*1.5 ± 0.1	A	0.45	0.10
CO2_8	0.24	1.53 ± 0.04	A	0.51	0.10
CO2_9	0.24	*1.5 ± 0.1	A	0.58	0.10
CH4_1	0.24	1.7 ± 0.2	C	0.46	3.50
CH4_2	0.24	1.9 ± 0.6	C	0.53	3.50
CH4_3	0.24	*1.5 ± 0.5	C	0.54	3.50
CH4_4	0.24	*1.5 ± 0.5	C	0.54	3.50
CH4_5	0.24	*1.5 ± 0.5	C	0.54	3.50
CH4_6	0.24	1.9 ± 0.6	C	0.64	3.50
CH4_7	0.24	1.3 ± 0.1	C	0.64	3.50
CH4_8	0.24	1.8 ± 0.2	C	0.73	3.50

2.2. Hydrate formation and permeability measurement

Brine-saturated cores were mounted into a rubber sleeve and placed inside a Hassler core holder (Fig. 1). All pump lines leading to the core (not the core itself) were purged under vacuum before filling the pumps with either CH_4 (> 99.5%) or CO_2 (> 99.999%) gas. The gas was introduced to the pore space at atmospheric pressure, and the pore pressure was then gradually increased by injecting gas from both ends: 8.3 MPa with CH_4 and 7.0 MPa with CO_2. The CH_4 remained gaseous throughout the experiments whereas the CO_2 was converted to liquid state during the pressure increase. The overburden pressure was continuously kept 3 MPa above the pore pressure. End-point relative permeability to CH_4 gas prior to hydrate formation was measured at steady-state (gas injection rate equal to gas production rate) with a maximum volumetric flow rate of 16 mL/min to avoid further de-saturation of the core. Injection pressure at the inlet, differential pressure across the core length, and core surface temperature at the inlet were recorded for three different flow rates to verify linearity between pressure drop and flow rate. The effective permeability to CH_4 was subsequently calculated by Darcy's law. The effective permeability to liquid CO_2 was not measured in each core prior to hydrate formation. Instead, CO_2-brine relative permeability curves were generated by draining a reference core initially saturated with brine. The core was gradually de-saturated with brine by incrementally increasing the volumetric flow rate of CO_2 and the effective permeability to liquid CO_2 was calculated by Darcy's law for each saturation step.

Hydrate formation was initiated by cooling the system to 4 °C by circulating antifreeze through a cooling jacket surrounding the core holder (Fig. 1). The volume of injected CH_4 or CO_2 needed to maintain constant pore pressure during hydrate formation was recorded and used to calculate the saturation of hydrate, see Almenningen et al. (2017) for details. A hydration number of 5.99 was used for CH_4 (Circone et al., 2005) and 6.4 for CO_2 (Henning et al., 2000). Less than a day of formation was typically required to complete CO_2 hydrate formation whereas CH_4 hydrate formation continued for up to ten days. The end-

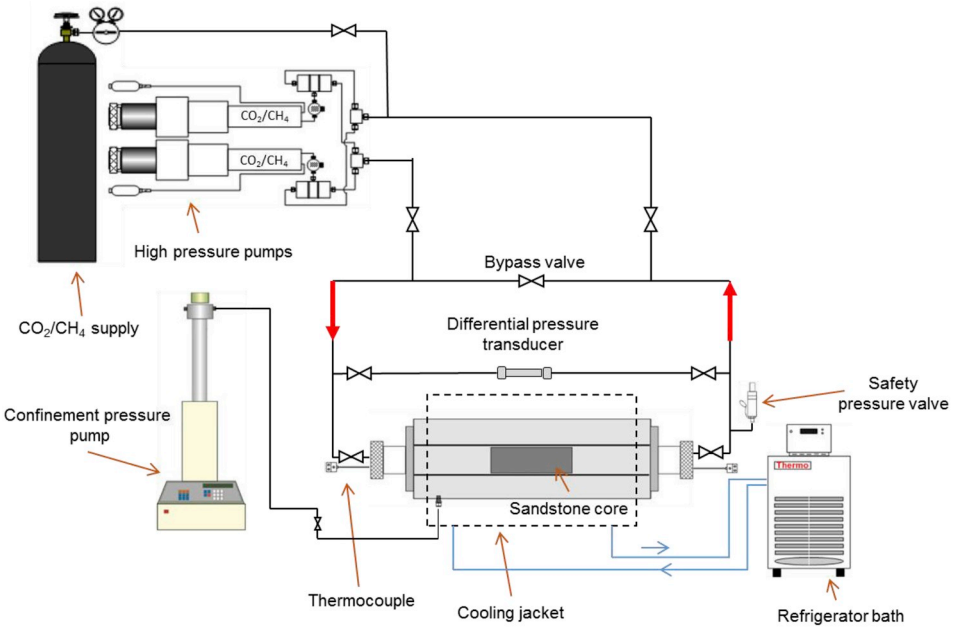

Fig. 1. Schematic of experimental design, modified from Hågenvik (2013). The core was mounted in a Hassler core holder and a net confinement pressure of 3 MPa was applied. The system temperature was maintained at 4 °C by circulating antifreeze through a cooling jacket surrounding the core holder. CH_4 or CO_2 were injected through the core from left to right, and the differential pressure was recorded and used to calculate the permeability.

point relative permeability (CH_4 or CO_2) was then measured by constant volumetric flow rate injection and a fixed outlet production pressure. Two separate high-pressure pumps were used for injection and production. The differential pressure used to calculate relative permeability was recorded at steady-state (gas injection rate equal to gas production rate), assuming constant fluid (hydrate, gas and water) saturations in the core. The differential pressure was monitored for several minutes after steady-state was achieved to verify the constant saturation assumption. No water production was observed during measurements. The injected CH_4 (or CO_2) was not precooled, but low volumetric injection rates allowed heat exchange between the CH_4 (or CO_2) and the cooled injection line leading into the core, and the inlet core temperature did not increase during the injection. Constant temperature at the inlet and outlet of the core also suggested no reformation or dissociation of hydrates during the flow period. However, localized hydrate phase transitions could not be ruled out without *in situ* monitoring of the pore space.

2.3. Calculation of fluid saturation

The fluid saturation (and water saturation) can be calculated either as a fraction of the original pore volume or as a fraction of the dynamic pore volume adjusted for hydrate growth. Both saturation definitions are used throughout the manuscript and are calculated as follow:

Constant pore volume

The fluid saturation is given as:

$$S_{CH4(or\ CO2)} = \frac{V_{CH4(or\ CO2)}}{V_{pore}} \quad (1)$$

where $V_{CH4\ (or\ CO2)}$ is the volume of gaseous CH_4 (or volume of liquid CO_2) and V_{pore} is the pore volume of the rock. The formation of hydrate is treated as an additional phase and the pore volume is saturated with the sum of three co-existing phases (CH_4 (or CO_2), water and hydrate):

$$V_{pore} = V_{CH4(or\ CO2)} + V_w + V_H \quad (2)$$

Dynamic pore volume

The solid hydrate is treated as an extension of the rock matrix and not as a separate phase in the pore space. The pore volume is then denoted as an effective pore volume and is given by the sum of two phases (CH_4 (or CO_2) and water):

$$V^*_{pore} = V_{pore} - V_H = V_{CH4(or\ CO2)} + V_w \quad (3)$$

The effective fluid saturation becomes

$$S^*_{CH4(or\ CO2)} = \frac{V_{CH4(or\ CO2)}}{V^*_{pore}} \quad (4)$$

3. Results and discussion

3.1. Initial brine distribution

The brine saturation and distribution in the core prior to hydrate formation were highly sensitive to the saturation method used (A, B or C), and the brine saturation varied along the length of the core as well as in the transverse direction (Figs. 2 and 3).

Saturation method A (De-saturation of a fully brine-saturated core by CO_2 injection at ambient conditions): This method resulted in a uniformly distributed brine saturation in every cross-section of the core (Fig. 2A). However, the brine saturation changed with the length of the core and was lowest at the inlet side where the CO_2 had been injected (Fig. 3). The brine saturation was increased at the outlet face of the core because of the capillary end-effect.

Saturation method B (Temporary spontaneous imbibition for 10–20 s): In this case, the longitudinal saturation values were consistent (Fig. 3), but the brine saturation varied in the transverse direction and was highest further away from the core center (Fig. 2B). The spontaneous imbibition took place radially inwards to the core center and the time-limited water supply resulted in a saturation gradient.

Saturation method C (Fully brine-filled core wrapped in paper and purged under vacuum for 10–20 s): This method yielded the most non-uniform saturation of brine. The brine saturation was highest in the center of the core and decreased radially outwards (Fig. 2C), opposite of the saturation gradient in method B. The saturation was also changing along the length of the core and the brine saturation was lowest in both ends of the core (Fig. 3).

The different outcome of brine saturation and distribution from the three methodologies highlights the difficulty associated with establishing a repeatable homogeneous initial saturation. The initial brine distribution is not of interest in itself, but a homogenous brine saturation will increase the likelihood of achieving a homogenous final hydrate saturation. This is desired to ensure consistency between runs and to correlate fluid permeability to hydrate and fluid saturation. The

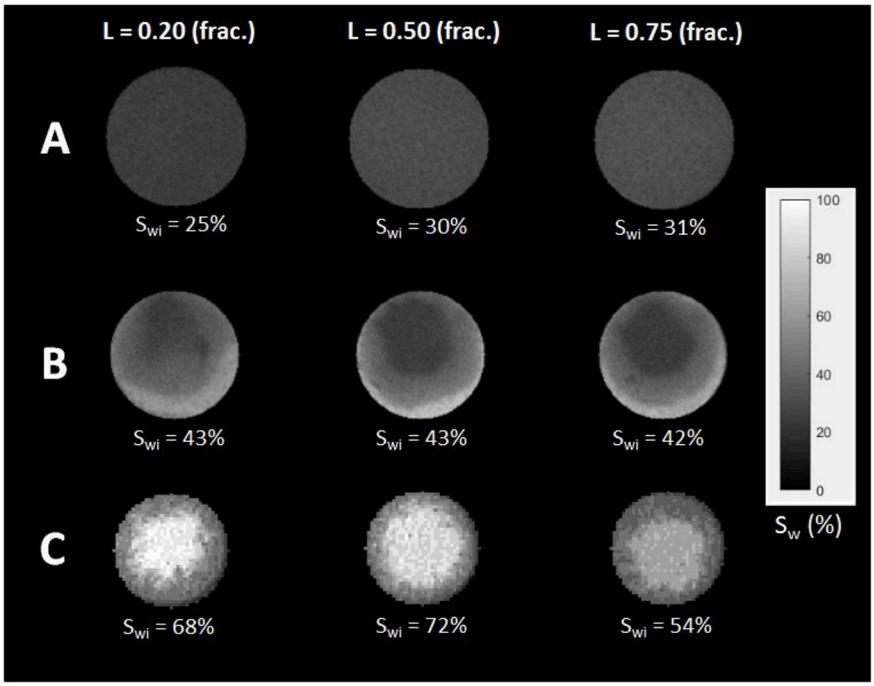

Fig. 2. Initial distribution of brine prior to pressurization by CH_4 (or CO_2) and subsequent hydrate formation. A: Core partially saturated with brine by CO_2 injection at ambient conditions into a 100% brine-filled core. B: Core partially saturated with brine by temporary (10–20 s) spontaneous imbibition. C: Core partially saturated with brine by vacuum-drainage of a 100% brine-filled core.

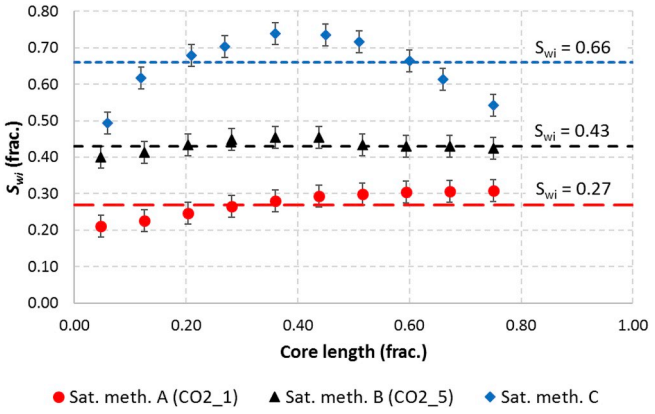

Fig. 3. Initial distribution of brine along the length of the core prior to pressurization by CH_4 (or CO_2) and subsequent hydrate formation. The average brine saturation is indicated with straight lines. Note that the core saturated by saturation method C (diamonds) are not part of the permeability experiments in this study (not included in Table 1).

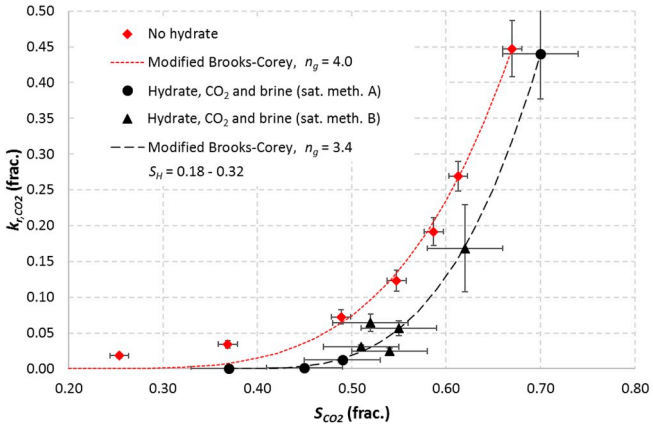

Fig. 4. Relative permeability values for liquid CO_2 as a function of CO_2 saturation. Two-phase permeability (diamonds) was obtained by draining brine at different flow rates in a single core. Three-phase permeability values represent individual cores where the hydrate saturation ranged from 0.18 to 0.32: Saturation method A in circles and saturation method B in triangles. The permeability values are fitted with modified Brooks-Corey curves based on least squares regression. Error bars reflect instrumental uncertainties.

extent of hydrate saturation heterogeneity within each core is not quantified in this experimental work, but discrepancies in measured permeability between experiments with the same fluid saturation may be attributed to changes in saturation distribution between runs.

3.2. Carbon dioxide relative permeability

CO_2 relative permeability values in Bentheim sandstone (Fig. 4) were measured with and without CO_2 hydrate present in the pore space. The former case is henceforth referred to as a three-phase system (CO_2 hydrate, liquid CO_2 and brine) whereas the latter case is referred to as a two-phase system (liquid CO_2 and brine). End-point $k_{r,CO2}$ measurements without CO_2 hydrate present used a single core plug (CO2_base) with different CO_2 flow rates to achieve a range in saturations (S_{CO2} = 0.25–0.67). End-point $k_{r,CO2}$ with CO_2 hydrate present were measured using different core plugs (see Table 2) with a range in CO_2 saturations (S_{CO2} = 0.37–0.70) and CO_2 hydrate saturations (S_H = 0.18–0.32). The relative permeability to CO_2 was consistently lower for the three-phase system than for the two-phase system for similar saturations of CO_2. The presence of solid hydrates clearly reduce the CO_2 permeability even if the CO_2 saturation is kept constant. The effect of the initial brine saturation method was limited as all of the three-phase permeability values follow the saturation consistently (Fig. 4), meaning that saturation method A and B can both be used as a starting point for hydrate formation experiments. The radial brine saturation gradient resulting from saturation method B did not influence the final hydrate distribution and thereby the permeability significantly compared to the hydrate distribution and permeability resulting from saturation method A.

The permeability curves were fitted with modified Brooks-Corey curves (Alpak et al., 1999):

$$k_{r,CO2} = k^0_{r,CO2}\left(\frac{S_{CO2} - S_{CO2r}}{1 - S_{CO2r} - S_{wr}}\right)^{n_g} \quad (5)$$

Table 2
List of every CO_2 permeability experiment. The core pressure and temperature were kept constant at 7.0 MPa and 4 °C, respectively, during hydrate formation and permeability measurements. Margin of errors reflect instrumental uncertainties.

Core ID	S_H (frac.) ± 0.04	S_{CO2} (frac.)	$k_{r,CO2}$ (frac.)
CO2_base	0	0.25 ± 0.01	0.018 ± 0.003
CO2_base	0	0.37 ± 0.01	0.034 ± 0.005
CO2_base	0	0.49 ± 0.01	0.07 ± 0.01
CO2_base	0	0.55 ± 0.01	0.12 ± 0.01
CO2_base	0	0.59 ± 0.01	0.19 ± 0.02
CO2_base	0	0.61 ± 0.01	0.27 ± 0.02
CO2_base	0	0.67 ± 0.01	0.45 ± 0.04
CO2_1	0.18	0.70 ± 0.04	0.44 ± 0.06
CO2_2	0.23	0.62 ± 0.04	0.17 ± 0.06
CO2_3	0.31	0.54 ± 0.04	0.025 ± 0.004
CO2_4	0.32	0.55 ± 0.04	0.06 ± 0.01
CO2_5	0.30	0.51 ± 0.04	0.031 ± 0.003
CO2_6	0.19	0.52 ± 0.04	0.06 ± 0.01
CO2_7	0.30	0.49 ± 0.04	0.012 ± 0.001
CO2_8	0.24	0.45 ± 0.04	0.00111 ± 0.00003
CO2_9	0.30	0.37 ± 0.04	0

where $k^o_{r,CO2}$ is end-point relative permeability to CO_2 at residual brine saturation S_{wr}, S_{CO2r} is residual saturation of CO_2, and n_g is a fitting parameter controlling the slope of the curve. A residual CO_2 saturation of 0.20 was assumed for the two-phase case and 0.37 when hydrate was present, based on the measured residual CO_2 saturations in this study. The best fit was achieved with $n_g = 4.0$ for the two-phase permeability values and $n_g = 3.4$ for the three-phase permeability values (Fig. 4). The corresponding normalized mean square error (NMSE) (Poli and Cirillo, 1993) was 0.23 and 0.02, respectively. Another form of the Brooks-Corey model that has previously been fitted to experimental CO_2-brine permeability data with $N_{CO2} = 2$–5 (Krevor et al., 2012), could not be fitted to the relative permeability values in this study. Notice that the hydrate phase was treated as an extension of the brine phase for the three-phase calculations, meaning that the sum of the brine and hydrate saturations were treated as one phase. Alternatively, the hydrate saturation is considered as a part of the solid matrix, giving scaled CO_2 and brine saturations according to the reduction of the pore volume. The absolute permeability of the porous medium is then a function of the dynamic porosity (Moridis and Pruess (2014) and references therein):

$$K = K_0\left(\frac{\Phi-\Phi_c}{\Phi_0-\Phi_c}\right)^n \quad (6)$$

where K_0 is the absolute permeability when the porosity is Φ_0 (no hydrate), Φ_c is a nonzero critical porosity where the absolute permeability becomes zero, and n is a fitting parameter that is dependent on where hydrate accumulates in the pore space. A value of n equal to 2.3 was chosen to calculate the absolute permeability of each core after hydrate formation, and the critical porosity was assumed to be 0.10 (frac.). The fitting parameter n was chosen as the maximum value that preserved the end-point relative permeability to CO_2 less than one (Fig. 5). A critical porosity of 0.10 corresponded to a critical hydrate saturation of 0.60, which was chosen since the CO_2 permeability became zero at a CO_2 saturation of 0.37. Now, the modified Brooks-Corey model gave the best fit to the measured relative permeability to CO_2 when n_g was set to 5.8 (Fig. 5) with a NMSE value of 0.15.

3.3. Methane relative permeability

The CH_4 permeability was measured as end-point permeability in different cores with different combinations of hydrate and fluid saturation (Table 3). The range in permeability values for the three-phase case was obtained for the CH_4 saturation interval of 0.18–0.44 and the CH_4 hydrate saturation ranged between 0.37 and 0.61. These measurements were first presented in Almenningen et al. (2016). Additional permeability values

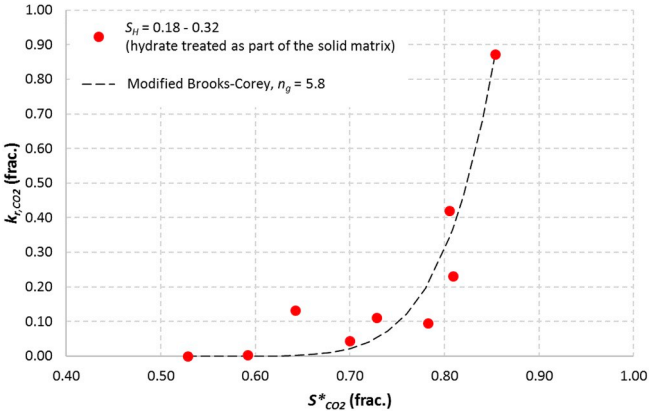

Fig. 5. Relative permeability to liquid CO_2 when hydrate is treated as part of the rock. The saturation of CO_2 (and brine) is scaled according to the reduction in porosity and the absolute permeability is scaled according to Eq. (6) with a fitting parameter $n = 2.3$. The permeability values are fitted with a modified Brooks-Corey curve based on least squares regression.

Table 3
List of all CH_4 permeability experiments. The core pressure and temperature were kept constant at 8.3 MPa and 4 °C, respectively, during hydrate formation and permeability measurements. Margin of errors reflect instrumental uncertainties.

Core ID	No hydrate		Hydrate		
	S_{CH4} (frac.) ± 0.01	$k_{r,CH4}$ (frac.)	S_H (frac.) ± 0.02	S_{CH4} (frac.) ± 0.02	$k_{r,CH4}$ (frac.)
CH4_1	0.54	0.12 ± 0.02	0.46	0.44	1.9E-2 ± 0.3E-2
CH4_2	0.47	0.19 ± 0.08	0.47	0.36	1.2E-3 ± 0.4E-3
CH4_3	0.46	0.09 ± 0.03	0.45	0.36	1.7E-6 ± 0.6E-6
CH4_4	0.46	0.06 ± 0.02	0.47	0.36	4E-6 ± 1E-6
CH4_5	0.46	0.06 ± 0.02	0.51	0.35	1.4E-4 ± 0.5E-4
CH4_6	0.36	0.08 ± 0.03	0.61	0.23	4E-7 ± 1E-7
CH4_7	0.36	0.14 ± 0.02	0.53	0.24	9.9E-7 ± 0.8E-7
CH4_8	0.27	0.032 ± 0.006	0.37	0.18	7.1E-7 ± 0.8E-7

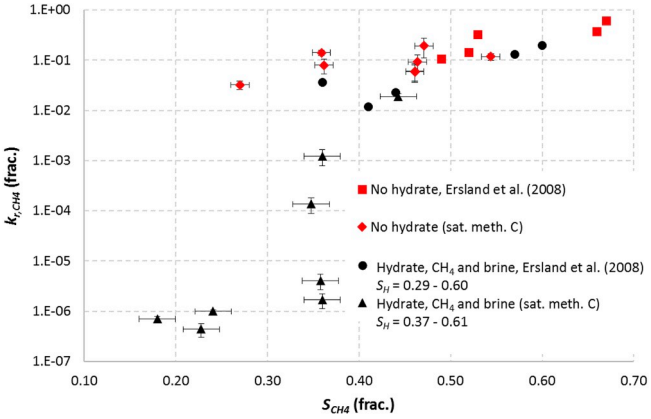

Fig. 6. Relative permeability values for CH_4 gas (logarithmic scale) as a function of CH_4 saturation. Two-phase permeability (diamonds and squares) was obtained on individual cores at room temperature prior to hydrate formation. Three-phase permeability values (triangles and circles) were measured on the same cores at 4 °C after hydrate formation. The hydrate saturation varied from 0.29 to 0.61 in the different cores. This plot was first presented in Almenningen et al. (2016), and some of the data points (squares and circles) are obtained from Ersland et al. (2008) (not included in Table 3). Error bars reflect instrumental uncertainties.

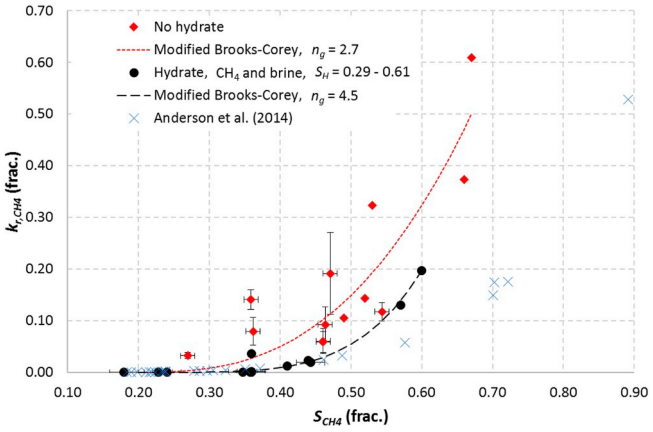

Fig. 7. Relative permeability values for CH_4 gas as a function of CH_4 saturation. Two-phase permeability (diamonds) was obtained on individual cores at room temperature prior to hydrate formation. Three-phase permeability values (circles) were measured on the same cores at 4 °C after hydrate formation. The hydrate saturation varied from 0.29 to 0.61 in the different cores. The permeability values are fitted with modified Brooks-Corey curves based on least squares regression. One data set from Anderson et al. (2014) is included for comparison. Error bars reflect instrumental uncertainties.

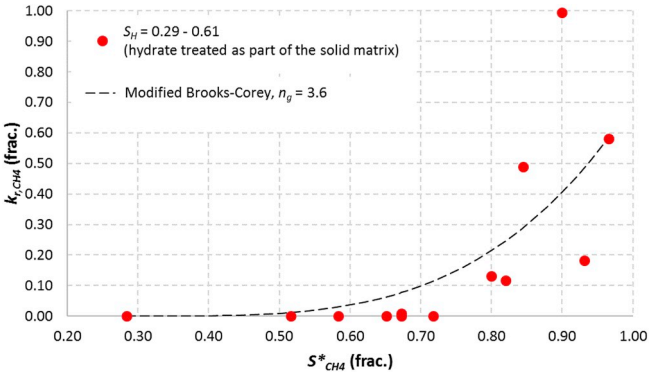

Fig. 8. Relative permeability to CH_4 gas when hydrate is treated as part of the rock. The saturation of CH_4 (and brine) is scaled according to the reduction in porosity and the absolute permeability is scaled according to Eq. (6) with a fitting parameter n = 1.7. The permeability values are fitted with a modified Brooks-Corey curve based on least squares regression.

from Ersland et al. (2008) were included to increase the size of the permeability sample (Fig. 6). A transition of significant loss of CH_4 relative permeability was observed in the CH_4 saturation range equal to 0.33–0.38 when the permeability values were plotted on a logarithmic scale (Fig. 6). In this saturation interval, the effective CH_4 permeability dropped from mD-scale to μD-scale. The three-phase permeability values were also consistently lower than the two-phase permeability values for gas saturations greater than 0.40 (Fig. 7). The addition of solid hydrates lowered the CH_4 permeability at constant CH_4 saturation, similar as for the CO_2 hydrate measurements. The permeability values were scattered, especially for the two-phase flow prior to hydrate formation (Fig. 7). Every core was initially saturated with brine by saturation method C, which was observed to give variations in brine saturation both radially and along the length of the core (Figs. 2 and 3). The scatter in permeability for the two-phase system could therefore be attributed to heterogeneities in the brine distribution. Permeability values obtained during the Iġnik Sikumi field trial (Anderson et al., 2014) are included for comparison in Fig. 7. The reported values from Anderson et al. (2014) are measure of the fluid mobility at given hydrate saturation, and the permeability values are included based on the assumption that the rest of the pore space was filled with CH_4 gas. If immobile water was present in addition to gas, the gas saturation would be less than what is assumed in Fig. 7 and the data points should shift leftwards.

Modified Brooks-Corey curves (Alpak et al., 1999) were compared with the permeability values based on a residual CH_4 saturation of 0.20 for both the two-phase case and when CH_4 hydrate was present. The best fit was achieved with n_g = 2.7 for the two-phase values and n_g = 4.5 for the three-phase values (Fig. 7). The corresponding normalized mean square error (NMSE) was 0.20 and 0.09, respectively. If the CH_4 hydrate saturation was treated as a part of the solid matrix, giving scaled fluid saturation and absolute permeability according to the reduction of available pore space, the permeability values were best matched with n_g = 3.6 (Fig. 8). A fitting parameter n = 1.7 and a critical porosity Φ_0 = 0.07 were used in Eq. (6). The increased scatter of the data points for CH_4 hydrate compared to CO_2 hydrate was reflected by the NMSE value which was equal to 1.09.

3.4. Comparison of results

The relative permeability to CH_4 was higher than the relative permeability to CO_2 in the saturation interval of $0.40 < S_{CH4\ (or\ CO2)} < 0.60$, both for two-phase flow and when hydrate resided in the pores. CO_2 was in liquid state at the operating pressure and temperature of 7.0 MPa and 4 °C, respectively, while CH_4 was a gas at 8.3 MPa and 4 °C. The CO_2 had consequently a much higher density and viscosity (ρ = 932 kg/m^3 and μ = 0.0001 Pa*s) compared to methane (ρ = 70 kg/m^3 and μ = 0.00001 Pa*s). The relative permeability to CO_2 became apparently zero at a CO_2 saturation of 0.37 (S_H = 0.30) as it was not possible to obtain any flow at this saturation. The relative permeability to CH_4 dropped significantly in the CH_4 saturation interval of 0.33–0.38, but not to the extent that the core became completely blocked. Low flow rates were measured down to a CH_4 saturation of 0.18 (S_H = 0.37). The different behavior between CH_4 and CO_2 may arise from the difference in physical state of the phases, and the low detectable flow rates of CH_4 at low CH_4 saturation could result from diffusive flow through the pore space.

The inclusion of solid hydrate in the pore space reduced the relative permeability to CH_4 and CO_2 compared to the two-phase system (no hydrate), at constant CH_4 (or CO_2) saturation. The combination of hydrate and brine in the pore space constituted more resistance to flow than brine alone. This may come of brine and hydrate occupying different parts of the pores. The residual water in the two-phase system will reside close to grain surfaces because of the water-wet grains in Bentheim sandstone, enabling CH_4 (or CO_2) to flow through the middle of the pores. Hydrate is previously shown to grow along the CH_4-water interface, encapsulating the gaseous CH_4 residing in the middle of pores (Almenningen et al., 2018). Many of the CH_4 flow paths are therefore blocked after hydrate has formed. The existence of completely immobile CH_4 (or CO_2) shielded by hydrates are likely the reason why the relative permeability is lower for the three-phase system compared to the two-phase system. A greater degree of the CH_4 (or CO_2) saturation is mobile when only CH_4 (or CO_2) and water are present in the pores. The same reduction in permeability is necessarily not true for other rock types with different wetting properties. If the rock was gas-wet, with water residing in the middle of pores, the hydrate layer formed at the interface would likely affect the gas permeability less than what is observed here. Caution should be exercised when comparing permeability values across rock samples with different mineralogy and unknown hydrate distribution.

The modified Brooks-Corey fitting exponent increased from 4.0 to 5.8 for CO_2 and from 2.7 to 3.6 for CH_4. Simulation results for CH_4 hydrate showed similarly that the fitting exponent increased from 2.6 for S_H = 0.2 to 3.5 for S_H = 0.6 (Mahabadi et al., 2016), and the fitting exponent in a modified Stone equation increased from 1.8 for S_H = 0.1 to 3.5 for S_H = 0.6 (Mahabadi and Jang, 2014). The reduction in relative permeability was quantified further by taking the ratio of the relative permeability to CH_4 (or CO_2) for the three-phase system and the relative permeability to CH_4 (or CO_2) for the two-phase system.

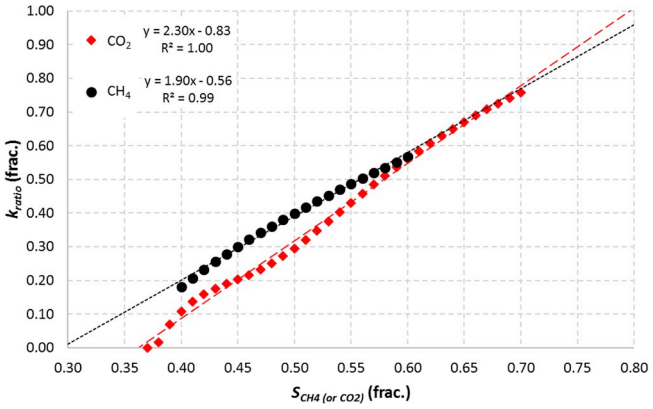

Fig. 9. Permeability ratios for CH_4 gas (circles) and liquid CO_2 (diamonds) as a function of CH_4 (or CO_2) saturation. The permeability ratio is here defined as the relative permeability to CH_4 (or CO_2) when hydrate is present (three-phase) divided by the relative permeability to CH_4 (or CO_2) without hydrate present (two-phase), for equal CH_4 (or CO_2) saturation for each ratio. The hydrate saturation ranged between 0.18 and 0.32 for the CO_2 measurements and 0.29 and 0.56 for the CH_4 measurements.

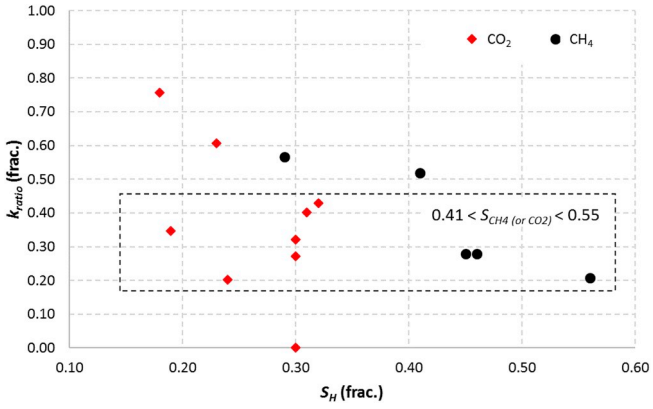

Fig. 10. Permeability ratios for CH_4 gas (circles) and liquid CO_2 (diamonds) as a function of hydrate saturation. The permeability ratio is here defined as the relative permeability to CH_4 (or CO_2) when hydrate is present (three-phase) divided by the relative permeability to CH_4 (or CO_2) without hydrate present (two-phase), for equal CH_4 (or CO_2) saturation for each ratio. The stapled rectangle highlights the limited effect of changing the hydrate saturation on the permeability ratio.

Each permeability ratio was calculated for the same CH_4 (or CO_2) saturation (Fig. 9):

$$k_{ratio}(S_{CH4(or\ CO2)}) = \frac{k_{r,CH4(or\ CO2)}(three-phase)}{k_{r,CH4(or\ CO2)}(two-phase)} \quad (7)$$

The relative permeability to CH_4 (or CO_2) was obtained for the entire saturation interval by interpolation between the measured relative permeability values. The resulting relation between the permeability ratio and CH_4 (or CO_2) saturation showed an increasing trend with saturation for both CH_4 and CO_2 (Fig. 9). The value of the ratio increased linearly with increasing CH_4 (or CO_2) saturation, demonstrating less difference between the two-phase system and the three-phase system for higher CH_4 (or CO_2) saturations. For instance, when the CO_2 saturation was higher than 0.62, the relative permeability of the three-phase system was within 60% of the relative permeability of the two-phase system. This means that the formed hydrate has impaired the CO_2 permeability with 40%, probably by a combination of complete immobilization of some of the CO_2 and by an increase in the tortuosity of the CO_2 flow path. When the CO_2 saturation was lower than 0.45, the relative permeability of the three phase system was at most 20% of the relative permeability of the two-phase system. The effective permeability of the CO_2 was more sensitive to hydrate formation at low CO_2 saturations, most likely because the limited CO_2 phase was more prone to become disconnected and capillary immobilized. The ratio between the two-phase and three-phase relative permeability to CH_4 was comparable to the CO_2 ratio and followed the same increasing trend with increasing CH_4 saturation.

The strong correlation between the ratio of relative permeability and CH_4 (or CO_2) saturation implicates that the actual hydrate saturation had limited effect on the permeability for a given CH_4 (or CO_2) saturation. This is highlighted when the permeability ratio was plotted against hydrate saturation (Fig. 10). The ratio of relative permeability did not change significantly when moving from a hydrate saturation of 0.19–0.56 as long as the CH_4 (or CO_2) saturation was fairly similar ($0.41 < S_{CH4\ (or\ CO2)} < 0.55$). For a given CH_4 (or CO_2) saturation, the presence of hydrate in addition to brine clearly reduced the effective permeability, but the mutual volumetric proportion between hydrate and brine was insignificant for the effective permeability for hydrate saturations lower than 0.56. The same conclusion is reached by investigating the effect of hydrate saturation on the relative permeability to CH_4 in the transitional CH_4 saturation zone between 0.33 and 0.38 (Fig. 11). The relative permeability to CH_4 was lower when hydrate was present in the pore space, but no reduction in permeability was

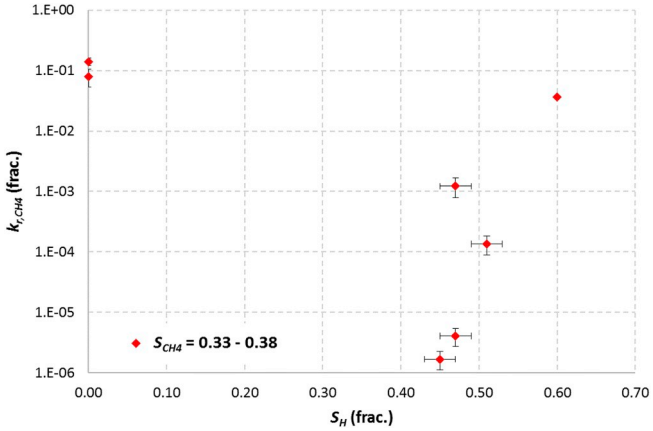

Fig. 11. Relative permeability to CH_4 as a function of hydrate saturation for constant CH_4 gas saturation. Error bars reflect instrumental uncertainties.

observed for increasing hydrate saturation. In fact, it seemed as if the relative permeability to CH_4 was increasing with increasing hydrate saturation for $S_{CH4} = 0.33–0.38$, albeit the spread in hydrate saturation was insufficient to conclude in general. Jaiswal et al. (2009) found two different trends for the change in relative permeability to CH_4 as a function of hydrate saturation when comparing two different core materials. A field sample demonstrated a decreasing relative permeability to CH_4 when the hydrate saturation increased from 0.07 to 0.31 (same trend for three different constant gas saturations of 0.20, 0.40 and 0.60). The same decrease in relative permeability to CH_4 was to the contrary not observed when the hydrate saturation increased from 0.05 to 0.36 in the other sample. The permeability values were more scattered and did not follow any particular trend. This shows that the relation between gas permeability and hydrate saturation remain unclear, and that it does not exist any general correlation between gas permeability and hydrate saturation for constant gas saturations. The effect of hydrate saturation on gas permeability will vary with the particular hydrate growth pattern and resulting hydrate distribution within the pores. The large change in relative permeability to CH_4 observed in the transitional CH_4 saturation (Fig. 11) indicates that it is difficult to reproduce the distribution of residual CH_4 gas after hydrate formation. Especially when the residual CH_4 saturation after hydrate formation is close to the critical CH_4 saturation needed to obtain flow. The effective permeability is then heavily affected by minor perturbations in the CH_4

distribution. The saturation method used to establish the initial brine saturation for the CH_4 experiments was the least successful method in achieving a homogenous brine distribution. Additional investigations into the effect of hydrate saturation on permeability alteration should be aided by *in situ* monitoring of the distribution of phases during flow.

4. Conclusions

This paper presents relative permeability to CH_4 and CO_2 in hydrate-bearing Bentheim sandstone core samples at reservoir conditions. The following conclusions are drawn:

- The relative permeability to CH_4 in a two-phase system without hydrates was higher than the relative permeability to CH_4 in a CH_4/brine/hydrate three-phase system, for similar CH_4 saturation. The modified Brooks-Corey exponent, n_g, increased from 2.7 to 3.6 when hydrate was present in the pore space.
- The relative permeability to CO_2 in a two-phase system without hydrates was higher than the relative permeability to CO_2 in a CO_2/brine/hydrate three-phase system, for similar CO_2 saturations. The modified Brooks-Corey exponent, n_g, increased from 4.0 to 5.8 when hydrate was present in the pore space.
- The observed reduction in permeability is believed to be related to an increase of immobile CH_4 (or CO_2) after hydrates have formed: A greater degree of the CH_4 (or CO_2) saturation is mobile when only CH_4 (or CO_2) and water are present in the pores.
- The relative reduction in permeability because of hydrates increased for decreasing CH_4 (or CO_2) saturation. The effective permeability of the CH_4 (or CO_2) was more sensitive to hydrate formation at low CH_4 (or CO_2) saturations, most likely because the limited CH_4 (or CO_2) phase was more prone to become disconnected and capillary immobilized.
- No correlation between permeability and hydrate saturation was found for constant CH_4 (or CO_2) saturation.

Acknowledgements

The authors would like to acknowledge Equinor for use of the MRI facility at Equinor's laboratories in Bergen. Some of the authors are indebted to the Research Council of Norway under Climit project: 255490.

Nomenclature

K_{abs}	absolute permeability (Darcy)
k_r^0	end-point relative permeability (frac.)
k_{ratio}	the ratio of the relative permeability to CH_4 (or CO_2) for the three-phase system and the relative permeability to CH_4 (or CO_2) for the two-phase system (frac.)
$k_{r,CH4}$	relative permeability to CH_4 (frac.)
$k_{r,CO2}$	relative permeability to CO_2 (frac.)
L	core length (frac.)
n	fitting parameter in permeability reduction formula (−)
n_g	fitting parameter in modified Brooks-Corey model (−)
S_{CH4}	saturation of methane (frac.)
S^*_{CH4}	effective saturation of methane (frac.)
S_{CO2}	saturation of carbon dioxide (frac.)
S^*_{CO2}	effective saturation of carbon dioxide (frac.)
S_g	saturation of gas (frac.)
S_H	saturation of hydrate (frac.)
S_r	residual saturation (frac.)
S_w	saturation of water (frac.)
S_{wi}	initial saturation of water (frac.)
V_{CH4}	volume of methane (mL)
V_{CO2}	volume of carbon dioxide (mL)
V_H	volume of hydrate (mL)
V_{pore}	pore volume (mL)
V^*_{pore}	effective pore volume (mL)
V_w	volume of water (mL)
Φ	porosity (frac.)

Appendix A. Supplementary data

Supplementary data to this article can be found online at https://doi.org/10.1016/j.petrol.2019.02.091.

References

Ahn, T., Lee, J., Huh, D.G., Kang, J.M., 2005. Experimental study on two-phase flow in artificial hydrate-bearing sediments. Geosystem Engineering 8 (4), 101–104. https://doi.org/10.1080/12269328.2005.10541244.

Almenningen, S., Flatlandsmo, J., Fernø, M.A., Ersland, G., 2017. Multiscale laboratory verification of depressurization for production of sedimentary methane hydrates. SPE J. 22 (01), 138–147. https://doi.org/10.2118/180015-PA.

Almenningen, S., Juliussen, H., Ersland, G., 2016. Permeability measurements on hydrate-bearing sandstone cores with excess water. In: Paper Presented at the 30th International Symposium of the Society of Core Analysts, Snowmass, Colorado, USA.

Almenningen, S., Iden, E., Fernø, M.A., Ersland, G., 2018. Salinity effects on pore-scale methane gas hydrate dissociation. J. Geophys. Res. Solid Earth 123 (7), 5599–5608. https://doi.org/10.1029/2017JB015345.

Alpak, F.O., Lake, L.W., Embid, S.M., 1999. Validation of a modified Carman-Kozeny equation to model two-phase relative permeabilities. In: Paper Presented at the SPE Annual Technical Conference and Exhibition, Houston, Texas, USA, . https://doi.org/10.2118/56479-MS.

Anderson, B., Boswell, R., Collett, T.S., Farrell, H., Ohtsuki, S., et al., 2014. Review of the findings of the iğnik Sikumi Co2-ch4 gas hydrate exchange field trial. In: Paper Presented at the 8th International Conference on Gas Hydrates, Beijing, China.

Circone, S., Kirby, S.H., Stern, L.A., 2005. Direct measurement of methane hydrate composition along the hydrate equilibrium boundary. J. Phys. Chem. B 109 (19), 9468–9475. https://doi.org/10.1021/jp0504874.

Dai, S., Kim, J., Xu, Y., Waite, W.F., Jang, J., et al., 2018. Permeability anisotropy and relative permeability in sediments from the national gas hydrate program expedition 02, offshore India. Mar. Petrol. Geol (in press). https://doi.org/10.1016/j.marpetgeo.2018.08.016.

Dallimore, S., Yamamoto, K., Wright, J.F., Bellefleur, G., 2012. Scientific results from the JOGMEC/NRCan/Aurora mallik 2007–2008 gas hydrate production Research well program, mackenzie delta, northwest territories, Canada, BulletinNo. 601. Natural Resources Canada.

Delli, M.L., Grozic, J.L.H., 2014. Experimental determination of permeability of porous media in the presence of gas hydrates. J. Pet. Sci. Eng. 120, 1–9. https://doi.org/10.1016/j.petrol.2014.05.011.

Ersland, G., Husebø, J., Graue, A., Kvamme, B., Baldwin, B., et al., 2008. Measurements of gas permeability and non-Darcy flow in gas-water-hydrate systems. In: Paper Presented at the 6th International Conference on Gas Hydrates, Vancouver, Canada.

Graue, A., Kvamme, B., Baldwin, B., Stevens, J., Howard, J.J., et al., 2008. MRI visualization of spontaneous methane production from hydrates in sandstone core plugs when exposed to CO2. SPE J. 13 (2), 146–152. https://doi.org/10.2118/118851-PA.

Henning, R.W., Schultz, A.J., Thieu, V., Halpern, Y., 2000. Neutron diffraction studies of CO2 clathrate Hydrate: formation from deuterated ice. J. Phys. Chem. A 104 (21), 5066–5071. http://doi.org/10.1021/jp0001642.

Hågenvik, C., 2013. CO2 Injection in Hydrate Bearing Sandstone with Excess Water. MSc. University of Bergen, Bergen, Norway.

Jaiswal, N.J., Dandekar, A., Patil, S., Hunter, R.B., Collett, T.S., 2009. Relative permeability measurements of gas-water-hydrate systems. Natural gas hydrates - Energy resource potential and associated geologic hazards: AAPG Memoir 89, 723–733. https://doi.org/10.1306/13201135M893366.

Jang, J., Santamarina, J.C., 2014. Evolution of gas saturation and relative permeability during gas production from hydrate-bearing sediments: gas invasion vs. gas nucleation. J. Geophys. Res. Solid Earth 119 (1), 116–126. https://doi.org/10.1002/2013JB010480.

Johnson, A., Patil, S., Dandekar, A., 2011. Experimental investigation of gas-water relative permeability for gas-hydrate-bearing sediments from the mount elbert gas hydrate stratigraphic test well, Alaska north slope. Mar. Petrol. Geol. 28 (2), 419–426. https://doi.org/10.1016/j.marpetgeo.2009.10.013.

Kleinberg, R.L., Flaum, C., Griffin, D.D., Brewer, P.G., Malby, G.E., et al., 2003. Deep sea NMR: methane hydrate growth habit in porous media and its relationship to hydraulic permeability, deposit accumulation, and submarine slope stability. J. Geophys. Res. Solid Earth 108 (B10), 1–17. https://doi.org/10.1029/2003JB002389.

Krevor, S.C.M., Pini, R., Zuo, L., Benson, S.M., 2012. Relative permeability and trapping of CO2 and water in sandstone rocks at reservoir conditions. Water Resour. Res. 48 (2), 1–16. http://doi.org/10.1029/2011WR010859.

Kumar, A., Maini, B., Bishnoi, P.R., Clarke, M., Zatsepina, O., Srinivasan, S., 2010. Experimental determination of permeability in the presence of hydrates and its effect on the dissociation characteristics of gas hydrates in porous media. J. Pet. Sci. Eng. 70 (1–2), 114–122. https://doi.org/10.1016/j.petrol.2009.10.005.

Kvamme, B., Graue, A., Buanes, T., Kuznetsova, T., Ersland, G., 2007. Storage of CO2 in natural gas hydrate reservoirs and the effect of hydrate as an extra sealing in cold aquifers. Int. J. Greenh. Gas Con. 1 (2), 236–246. https://doi.org/10.1016/S1750-

5836(06)00002-8.
Mahabadi, N., Dai, S., Seol, Y., Jang, J., 2019. Impact of hydrate saturation on water permeability in hydrate-bearing sediments. J. Pet. Sci. Eng. 174, 696–703. https://doi.org/10.1016/j.petrol.2018.11.084.
Mahabadi, N., Dai, S., Seol, Y., Yun, T.S., Jang, J., 2016. The water retention curve and relative permeability for gas production from hydrate-bearing sediments: pore-network model simulation. Geochem. Geophys. Geosyst. 17 (8), 3099–3110. https://doi.org/10.1002/2016GC006372.
Mahabadi, N., Jang, J., 2014. Relative water and gas permeability for gas production from hydrate-bearing sediments. Geochem. Geophys. Geosyst. 15 (6), 2346–2353. http://doi.org/10.1002/2014GC005331.
Milkov, A.V., 2004. Global estimates of hydrate-bound gas in marine sediments: how much is really out there? Earth Sci. Rev. 66 (3–4), 183–197. https://doi.org/10.1016/j.earscirev.2003.11.002.
Moridis, G.J., Pruess, K., 2014. User's Manual of the Tough+ Core Code v1.5: A General-Purpose Simulator of Non-isothermal Flow and Transport through Porous and Fractured Media. Lawrence Berkeley National Laboratory, USA Report LBNL-6871E. Retrieved from.
Moridis, G.J., Kowalsky, M.B., Pruess, K., 2007. Depressurization-Induced gas production from class-1 hydrate deposits. SPE Reservoir Eval. Eng. 10 (5), 458–481. https://doi.org/10.2118/97266-PA.
Poli, A.A., Cirillo, M.C., 1993. On the use of the normalized mean square error in evaluating dispersion model performance. Atmos. Environ. Part A. General Topics 27 (15), 2427–2434. https://doi.org/10.1016/0960-1686(93)90410-Z.
Reagan, M.T., Moridis, G.J., Zhang, K., 2008. Sensitivity analysis of gas production from class 2 and class 3 hydrate deposits. In: Paper Presented at the Offshore Technology Conference, Houston, USA, . https://doi.org/10.4043/19554-MS.
Schoderbek, D., Martin, K.L., Howard, J.J., Silpngarmlert, S., Hester, K., 2012. North slope hydrate fieldtrial: CO2/CH4 exchange. In: Paper Presented at the OTC Arctic Technology Conference, Houston, USA, . https://doi.org/10.4043/23725-MS.
Seol, Y., Kneafsey, T.J., 2011. Methane hydrate induced permeability modification for multiphase flow in unsaturated porous media. J. Geophys. Res. Solid Earth 116 (B8), 1–15. https://doi.org/10.1029/2010JB008040.
Servio, P., Englezos, P., 2001. Effect of temperature and pressure on the solubility of carbon dioxide in water in the presence of gas hydrate. Fluid Phase Equilib. 190 (1), 127–134. https://doi.org/10.1016/S0378-3812(01)00598-2.
Servio, P., Englezos, P., 2002. Measurement of dissolved methane in water in equilibrium with its hydrate. J. Chem. Eng. Data 47 (1), 87–90. https://doi.org/10.1021/je0102255.
Tohidi, B., Yang, J., Salehabadi, M., Anderson, R., Chapoy, A., 2010. CO2 hydrates could provide secondary safety factor in subsurface sequestration of CO2. Environ. Sci. Technol. 44 (4), 1509–1514. https://doi.org/10.1021/es902450j.
Yamamoto, K., Terao, Y., Fujii, T., Ikawa, T., Seki, M., et al., 2014. Operational overview of the first offshore production test of methane hydrates in the Eastern Nankai Trough. In: Paper Presented at the Offshore Technology Conference, Houston, Texas, USA, . https://doi.org/10.4043/25243-MS.